European Review for Medical and Pharmacological Sciences 2022; 26: 7349-7358

Swept-source endoscopic optical coherence tomography real-time imaging system based on GPU acceleration for axial megahertz high-speed scanning

J. LYU[1,2,3], L. REN[4,5], Q.-Y. LIU[2,3], Y. WANG[2,3], Z.-Q. ZHOU[1,2,3], Y.-Y. CHEN[2,3], H.-B. JIA[1,2,3], Y.-G. TANG[1,2,3], M. LI[1,2,3]

[1]Division of Life Sciences and Medicine, School of Biomedical Engineering (Suzhou), University of Science and Technology of China, Suzhou, China
[2]Suzhou Institute of Biomedical Engineering and Technology, Chinese Academy of Sciences, Suzhou, China
[3]Jiangsu Key Lab of Medical Optics, Suzhou Institute of Biomedical Engineering and Technology, Chinese Academy of Sciences, Suzhou, China
[4]School of Physical Science and Technology, [5]Advanced Institute for Brain and Intelligence, Guangxi University, Nanning, China

Abstract. – OBJECTIVE: In order to solve the problem of image real-time processing and correction for high-speed endoscopic swept-source optical coherence tomography (SS-OCT), we highly optimize a computer-unified device architecture-based platform and use a field-programmable gate array to summarize the application experience.

MATERIALS AND METHODS: We use the Half-Sync/Half-Asyn mode to optimize memory in order to build a high-throughput data thread pool for CPU. We use asynchronous streaming architecture to multiplex multiple threads at high speed to accelerate data processing. At the same time, we design a rotary scanning position information encoding feedback module to suppress image drift, which can realize 25ns logic-timing sequence synchronization control through FPGA 40MHz clock.

RESULTS: The maximum complete attainable axial-scan-processing rate (including memory transfer and display of B-scan frames) is 3.52 MHz for a 16-bit pixel depth and A-scans/s of 1024 pixels. To our knowledge, this is the fastest processing rate reported to date with a single-chip graphical processing unit for SS-OCT. Finally, the established high-speed SS-OCT is used to image mouse esophagus and human fingers, and the output images are stable. When the image size is 1024 × 1024 pixels, the real-time imaging rate is 200 frames per second.

CONCLUSIONS: This paper develops a real-time image processing and reconstruction technology suitable for high-throughput SS-OCT systems, which can have high-density operation and efficient parallelism, while suppressing high-speed image drift. It lays the foundation for the non-destructive, *in vivo*, non-staining, fast and convenient early tumor diagnosis of high-speed endoscopic SS-OCT.

Key Words:
Swept-source, Optical coherence tomography, GPU acceleration, Axial megahertz scanning, Field-programmable gate array, Suppress the image drift.

Introduction

Optical coherence tomography (OCT) is a real-time, *in vivo*, high-sensitivity, high-resolution, and non-invasive optical imaging method for biological tissues. It has a spatial resolution of 2-10 μm and an imaging range of 1-3 mm, and its lateral resolution and imaging depth are between that of an ultrasound scanner and a microscope[1,2]. Since the advent of endoscopic OCT[3], it has been rapidly developed and widely used in the diagnosis of gastroenteropathy, respiratory disease, gastrointestinal tumors, cardiovascular disease, lymphatic system disease, bile duct occlusion, and coronary artery blockage[4-13].

Real-time, high-speed imaging has become increasingly more important and urgent for endoscopic OCT systems. High-speed imaging can not only allow doctors to observe certain rapid physiological activities in real time with high resolution, such as blood flow[14,15], but also reduce

Corresponding Authors: Min Li, Ph.D; e-mail: limin@sibet.ac.cn; Yuguo Tang, Ph.D; tangyg@sibet.ac.cn

motion artifacts[16]. In the past 30 years, the scanning rate of a swept light source has increased from hundreds of kilohertz to the upper hundreds of megahertz range (i.e., 400 MHz) 17-22, which promotes the improvement of the imaging speed of OCT. At the same time, it also poses technical challenges for real-time data processing and image display. For swept-source optical coherence tomography (SS-OCT) systems, in particular, the real-time processing speed of a large amount of OCT data largely determines the imaging speed of the OCT system. Data processing mainly includes a windowing function, spectrum transformation, logarithmic computation, and normalization. Imaging speeds can only be increased if each data processing process is effectively accelerated.

In recent years, with the rapid development of graphical processing units (GPUs), the computing power and internal transmission bandwidth of GPUs have gradually increased. The use of GPUs for OCT data processing has become almost routine[23-26], enabling the development of low-cost OCT systems[27]. However, to realize real-time processing for OCT systems with faster sweep rates, such as megahertz OCT systems[28,29], GPU algorithms or architectures must be optimized[30]. For example, Jian et al[31] achieved OCT with a maximum complete attainable axial-scan-processing rate of 2.24 MHz after optimizing a GPU architecture.

In addition to imaging speed, imaging quality is another key technical parameter for SS-OCT systems, especially for rotating-optical-fiber endoscopic SS-OCT systems[32]. Since the rotation speed of the rotating-optical-fiber imaging probe is not constant, the number of A-scans between frames varies, resulting in the drift of SS-OCT images[33,34]. Therefore, it is particularly important to improve the imaging performance of SS-OCT systems to ensure image stability while improving the processing rate.

In this paper, we present our recent work on the development of a high-speed swept-source rotating-optical-fiber endoscopic SS-OCT system based on GPU-accelerated image reconstruction and a field-programmable gate array (FPGA) to suppress image drift. We eliminate the most time-consuming aspect of traditional methods – repeated memory creation and release – and optimize the bidirectional memory transmission between host and device. Furthermore, based on the hardware feedback signal, we use the high-speed logic operation of the FPGA under a 40-MHz clock to effectively suppress image drift and achieve a stable image display.

Materials and Methods

System Description

The SS-OCT system uses the Michelson interference principle to detect the weak reflective signal of the sample and the Fourier-transform principle to reconstruct the sample structure, as shown in Figure 1.

The beam of the broadband light source is divided into two beams by the fiber coupler; one is directed to the sample arm and the other to the reference arm. The backscattered light from the sample arm and the reflected light from the reference arm meet at the fiber coupling to form interference fringes. The system obtains multiple A-scans by performing a rotating scan (B-scan), and then, reconstructs a two-dimensional image *via* data processing. In the data-processing process, the asynchronous flow structure of the GPU is used for zero-padding, windowing, execution of a fast Fourier transform (FFT), logarithmic computation, normalization, and polar coordinate transformation. It hides the consumption of host transfer to device (H2D) transmission and does not need to send the data back to the computer, which greatly improves the GPU processing speed. Moreover, an FPGA is used to perform a high-speed logic operation under a 40-MHz clock and produce an update trigger signal to trigger the acquisition device. The entire process has the same clock timing to ensure accurate synchronous operation of every process. The linear-k sweep-frequency laser-light source ($\lambda 0$ = 1310 nm, $\Delta\lambda$ = 110 nm, AXSUN, USA) used in this study has a scanning frequency of 200 kHz, and the maximum sampling rate of the data-acquisition card (12-bit dual-channel, ATS-9373, Alazartech, Canada) used in this study can reach 4 GS/s; both the capture card and GPU use a PCIe Gen3 x16 interface for memory transfer with the central processing unit (CPU). The endoscopic probe is mainly composed of single-mode optical fiber and GRIN lens, with a diameter of 1.2 mm, the final axial resolution of the system is 7.3 μm, the actual imaging depth of the system in the air is 4.5 mm, and the highest sensitivity is 110dB. The working distance is 1.7 mm.

GPU Data-Processing Methods

The limiting factor in the previously reported GPU implementation of OCT data processing was the overhead of the memory transfer between the CPU host RAM and the GPU device off-chip global memory. Faced with the high-throughput data generated by the system, our strategy is to parallelize

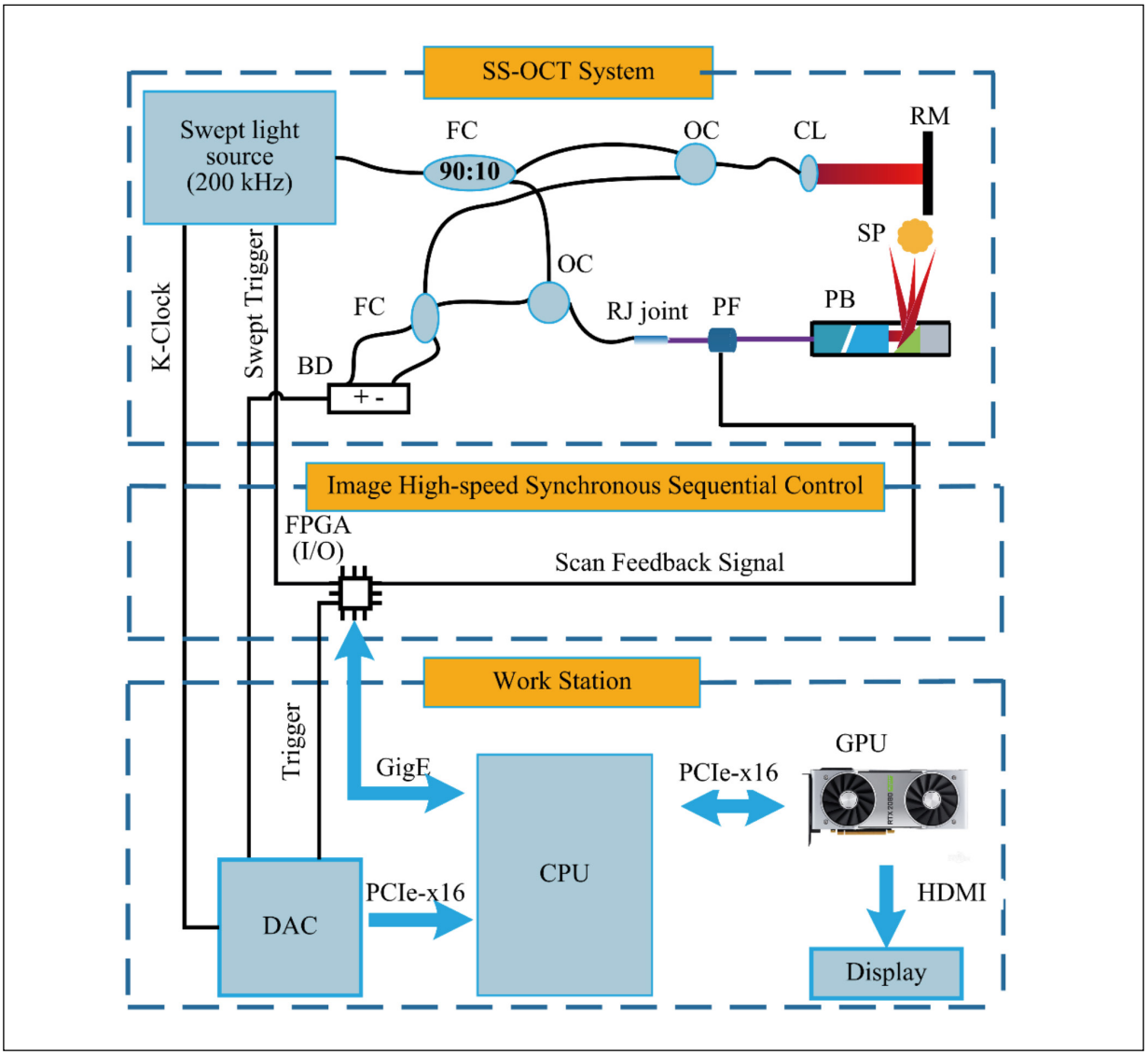

Figure 1. Schematic of SS-OCT system based on FPGA and GPU. BD, balanced detector; CL, collimator; DAC, data acquisition card; FC, fiber coupler; FPGA, field-programmable gate array; GigE, Gigabit Ethernet; GPU, graphical processing unit; HDMI, high-definition multimedia interface; OC, optical circulator; PB, probe; PCIe-x16, PCI Express x16 interface; PF, position feedback; RM, reference mirror; SP, sample.

the data transfer from the host to the device through the processing core to hide the memory transfer latency. Firstly, we use the constructor of the C++ class to initialize GPU variables and the destructor to complete the automatic release of GPU memory. Then, we use the member function of the C++ class and asynchronous flow architecture. By allocating page lock memory for the original data on the host side, we realize the asynchronous operation of the CPU and GPU, which hides the H2D time consumption. Finally, we call OpenGL to display the image directly on the GPU by computer unified device architecture (CUDA).

The specific architecture is shown in Figure 2A. The first sequence structure uses the C++ class constructor to initialize CUDA variables, including other variables (original interference signal data, FFT variables), window-function constants, binding CUDA stream, and CUDA fast Fourier transform (cuFFT) plan. The second sequence structure has a cyclic structure. First, two threads are created on the CPU side, one for raw data collection and the other for data transmission. The current-frame B-scan image is then split into two frames on the device side, which are put into two CUDA streams for synchronization process-

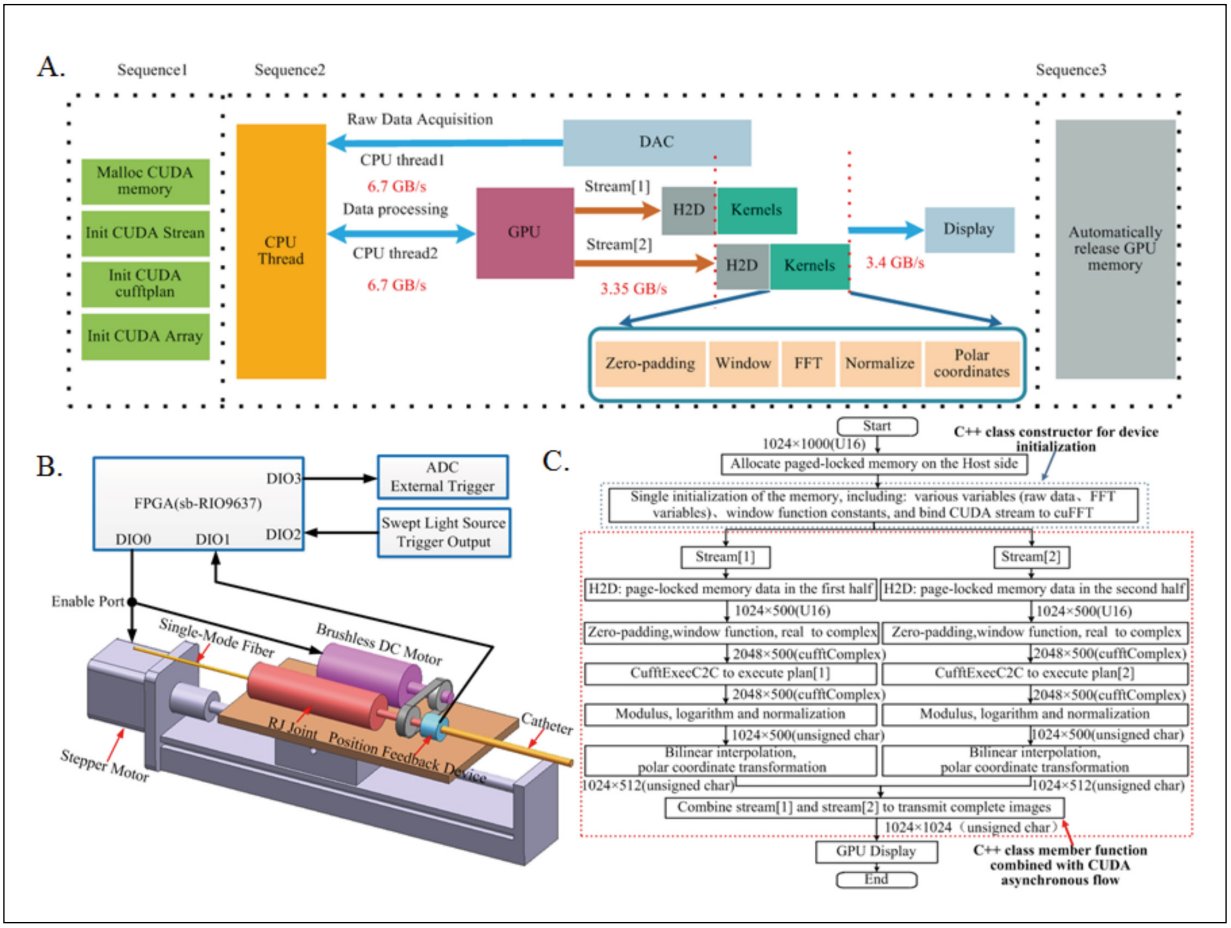

Figure 2. A, Data-processing architecture. CPU, central processing unit; DAC, data acquisition card; CUDA, computer unified device architecture; FFT, fast Fourier transform; GPU, graphical processing unit; H2D, host transfer to device. **B,** Specific processing method. FFT, fast Fourier transform; CUDA, computer unified device architecture; GPU, graphical processing unit; H2D, host transfer to device. **C,** System logic control diagram. DAC, data acquisition card; DC, direct current.

ing. Finally, OpenGL is used for image display. The third sequence structure automatically releases the memory to avoid GPU memory overflow caused by forgetting to release the memory.

Combined with the established high-speed SS-OCT system, the GPU data-specific processing method is depicted in detail in Figure 2B. When the size of each B-scan frame (original data) collected by the acquisition card is 1024 × 1000 pixels, the page-locked memory is allocated for the original data at the host end to improve the transmission speed of the host end between device ends. Then, the C++ class constructor is used to initialize GPU variables and bind CUDA stream [1] and stream [2] and cuFFT plan [1] and plan [2]. The original data are then divided into two 1024 × 500 data streams through H2D, which are put separately into stream [1] and stream [2], and then, the two data streams carry out operations, such as zero-padding, windowing, FFT, logarithmic computation, normalization, and polar-coordinate transformation at the same time. In addition, the algorithms as a universal method are also applied to other FDOCT systems. After the two data streams are completed, they are merged and displayed by the GPU using OpenGL. The key point of the above process is that the transmission between the host and device is hidden or eliminated, which is the benefit of using asynchronous flow.

FPGA Suppression of Image Drift

When endoscopic SS-OCT performs high-speed imaging, the rotation mechanism would be unstable due to the increase of rotating speed, resulting in the change of the number of A-scans between frames under the condition of non-uniform rotation distortion (NURD), which would eventually lead to

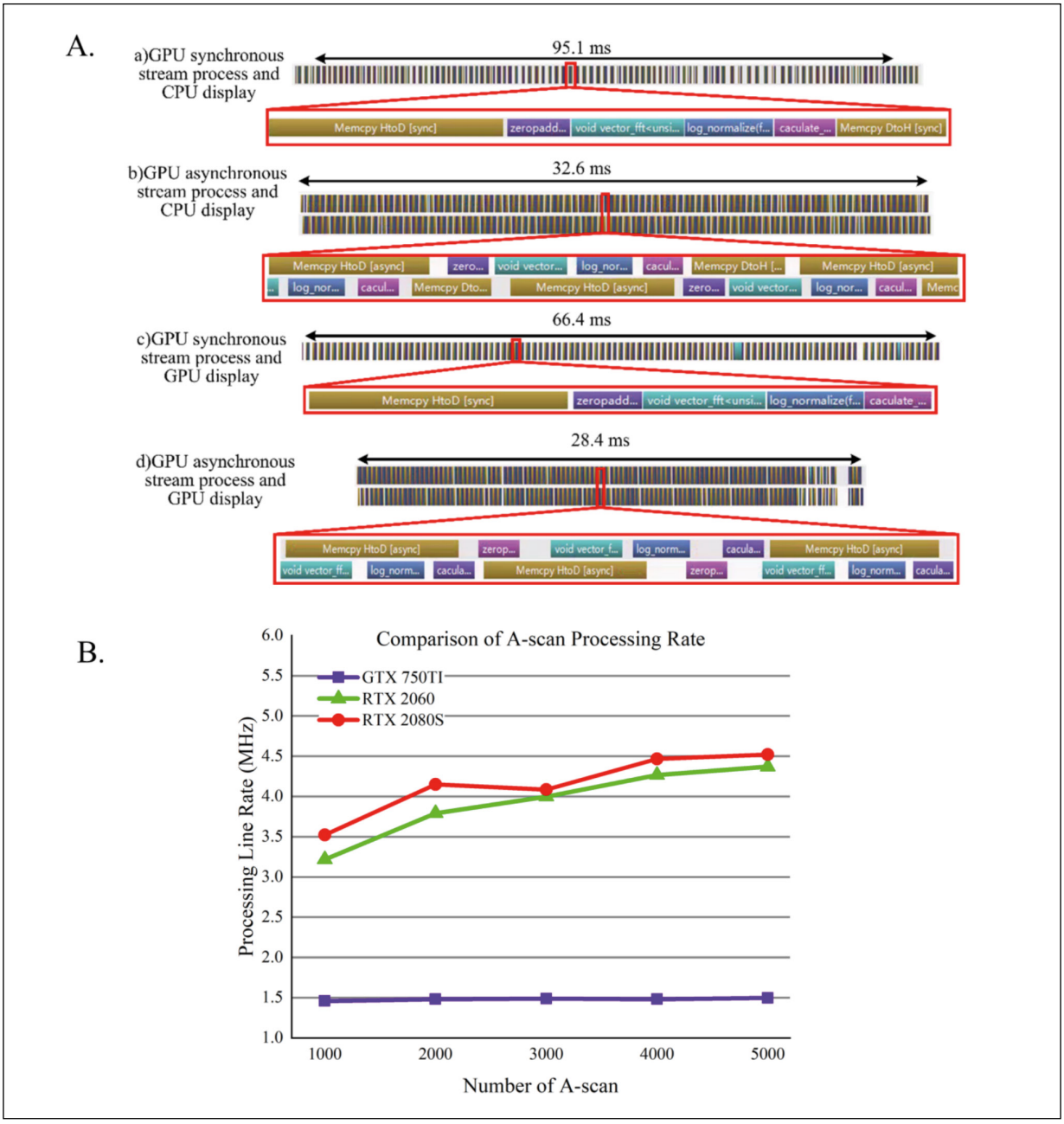

Figure 3. *A,* Total time for processing and image display for CPU and GPU in different modes. *B,* The graphics card processing rates for different A-scan sizes.

the phenomena of image drift, dragging, and so on. Therefore, we choose an FPGA card (sb-RIO9637, National Instruments, Austin, TX, USA) with an I/O function for high-speed image logic-timing sequence control. This card can make the rotating probe, swept-frequency light source, and acquisition card all be precisely and synchronously triggered.

As shown in Figure 2C, when the system starts to work, the FPGA outputs a high-level signal by DIO0 and makes the C-scan (z-axis scan) and B-scan (rotating scan) move synchronously. At the same time, the FPGA performs a logical "and" operation between DIO1 (the position feedback signal from the feedback device) and DIO2 (the swept-frequency trigger signal) at a frequency of 40 MHz of the basic clock, which means that synchronous logic-timing sequence control is performed every 25 ns. Then, high-speed logic-tim-

Table I. Comparison of several high-speed OCT imaging system.

Source	Raw line rate (kHz)	Depth scan size (number of voxels)	Frame size (number of scans)	OCT system speed (kHz)
Wei et al[24]	50	512	2048	128
Huang et al[26]	70	1024	1000	249
Choi et al[29]	2500	160	256	786
Wieser et al[30]	3216	400	320	2611
Jian et al[31,32]	100	256	2048	2240
Present paper	200	1024	1000	3520

ing sequence control results are synchronously triggered by the DIO3 output to the acquisition card for acquisition.

Results

Data-Analysis Results

As shown in Figure 3A, we use an RTX 2080 SUPER graphics card (NVIDIA, USA) to test 100 offline frames of 1000 × 1024 mouse colorectal data, and we use the CUDA Toolkit (64-bit, version 10.2) and NVIDIA driver for 64-bit Windows 10 in Microsoft Visual Studio 2017 as the development environment. The processing includes transmitting data from the host to the device, processing data from the device, and displaying the polar-coordinate transformation results. The processing algorithms include zero-padding, windowing, FFT, normalization, and polar-coordinate transformation. The results shown in Figure 3A include the following: (a) total consumption time of 95.1 ms by using GPU synchronous stream processing and CPU display, (b) total consumption time of 32.6 ms by using GPU asynchronous stream processing and CPU display, (c) total consumption time of 66.4 ms by using GPU synchronous stream processing and GPU display, and (d) total consumption time of 28.4 ms by using GPU asynchronous stream processing and GPU display. Among the aforementioned four modes, using GPU asynchronous stream processing and GPU display achieves the fastest processing speed. According to the calculation parameters of this mode, 100 frames consume 28.4 ms, and there are 1000 A-scans per frame used to calculate the image A-scan (16-bit, 1024 pixels) processing rate, which reaches up to 3.52 MHz.

To further study the influence of different A-scan sizes on the processing rate of graphics cards, we select the processing rates of different graphics cards at different speeds. Since the A-scan sizes generated by different speeds are different, the conversion relationship is as follows:

$$A-scan = \frac{rpm}{60} + \frac{1}{F_S} \quad (1)$$

In (1), A-scan is the number of line scan points, rpm is the motor speed per minute, and Fs is the sweep source frequency of 200 kHz.

Figure 3B shows the graphics card processing rates for different A-scan sizes, including memory transfer and image display. It can be seen that as the number of A-scans increases, the processing rate also increases. When the brushless motor speed is 12000 rpm (the corresponding A-scan number is 1000), and the fastest processing speed of A-scan (16 bit, 1024 pixels) reaches 3.52 MHz.

Table I shows a comparison of the achievements of the current work and previous works on real-time OCT. In many cases, data acquisition is the technical bottleneck. It can be seen from the table that the fastest A-scan processing rate reported by other researchers is 2.61 MHz. After optimizing system memory and using asynchronous stream architecture, the image A-scan (16-bit, 1024 pixels) processing rate reaches up to 3.52 MHz (including polar transformation processing), which is approximately 34.8% higher than the previous fastest processing rate.

Suppressed Image-Drift Results

To verify that the FPGA can suppress image drift, we perform rotation scanning imaging on a plane, set the acquisition speed to 100 fps, continuously record 100 frames of images, and mark the angle offset of the same point position with logic-timing sequence control and without logic-timing sequence control. The results are shown in Figure 4A.

Figure 4A shows the FPGA logic timing sequence results. Figure 4B shows the state after the

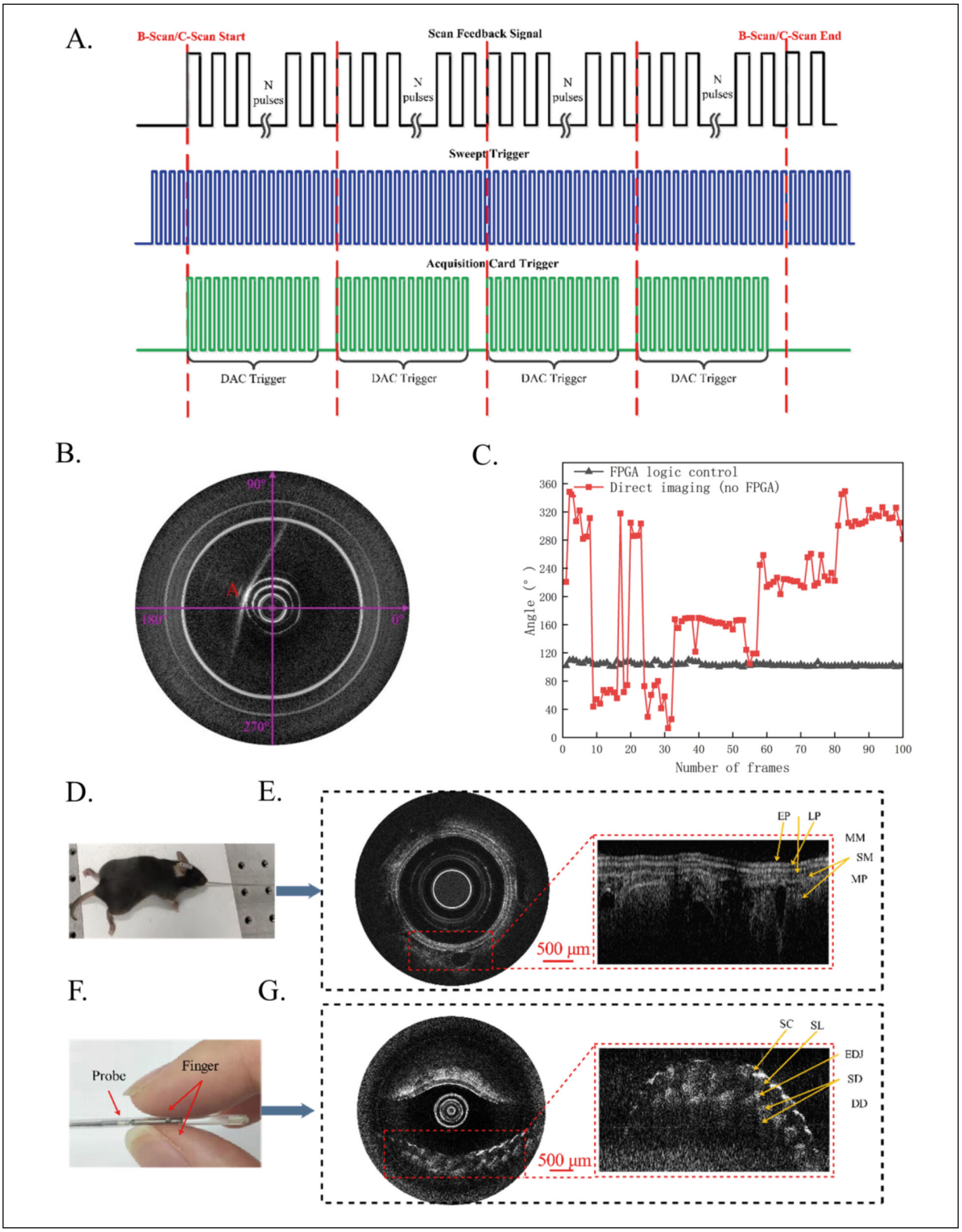

Figure 4. A, FPGA logic-timing sequence control diagram. DAC, data acquisition card; FPGA, field-programmable gate array. ***B,*** The coordinate system used to establish the angle of the same target at different positions. ***C,*** Results with and without FPGA logic-timing sequence control. (**D**) and (**E**) Esophagus structure of a living mouse. (**F**) and (**G**) Human finger structure. DD, deep dermis; EDJ, epidermal-dermal junction; EP, epithelium; LP, lamina propria; MM, muscularis mucosae; MP, muscularis propria; SC, stratum corneum; SD, superficial dermis; SL, stratum lucidum; SM, submucosa.

establishment of the coordinate system, real-time imaging, and marking the A-point angle offset. Figure 4C shows the imaging results of two methods. Without FPGA logic-timing sequence control, the maximum offset angle of the A point is 207.63°, and the minimum offset angle is 0.75°. With FPGA logic-timing sequence control, the maximum offset angle of the A point is 5.11° and the minimum offset angle is 0.02°. Therefore, adding high-speed logic-timing sequence control can effectively suppress image drift.

SS-OCT Tissue Imaging Results

The designed SS-OCT system is used to perform imaging experiments on a mouse esophagus and human fingers. The key parameters of the system are as follows: (1) the diameter of the endoscopic probe is 1.2 mm; (2) the axial resolution of the system is 7.3 μm; (3) the actual imaging depth of the system in the air is 4.5 mm; (4) the highest sensitivity is 110 dB; and (5) the acquisition rate is 100 fps. The data obtained by the system are processed by GPU and then denoised by wavelet transform, which can effectively distinguish the mutation and noise in the signal to achieve the purpose of noise reduction. The final results are shown in Figure 4D-G. Figure 4D shows how the rotating endoscopic probe is inserted into an experimental mouse, and 4E shows the resulting esophageal diagrams of the living mouse. Figure 4F shows how the rotating endoscopic probe is positioned relative to human fingers, and 4G shows the resulting images of the human fingers. The experimental results clearly show the structure of each layer of the mouse esophagus and human fingers. During the biological experiment, a series of measures such as anesthesia is taken to reduce harm to the mouse. All operations were approved by the experimental animal ethics committee of Suzhou Institute of Biomedical Engineering and Technology, Chinese Academy of Sciences, and met the requirements of the management methods of experimental animals in Jiangsu Province, China.

Discussion

Improving the imaging speed of swept-source endoscopic OCT has always been the goal pursued by scholars around the world. Since a faster imaging speed can observe some fast physiological activities in real-time and with high temporal resolution. For example, it is of great significance for the pathological diagnosis of cardiovascular diseases, such as heart disease and the online detection of living biological tissues. When the imaging speed of OCT is greater than the physiological motion speed of the tissue, motion artifacts can be reduced, the diagnosis time of patients can be shortened, and the diagnosis efficiency can be improved. It is worth noting that swept-frequency OCT will make the rotating mechanism unstable due to the increase of rotation speed during high-speed imaging. As a result, the number of A-line scans between frames will change under the condition of non-uniform rotation distortion, which will eventually lead to image drift and dragging. Therefore, it is necessary to consider how to improve the imaging speed of the OCT system while ensuring stable image output.

In response to the problem of imaging speed, international scholars have tried to use GPUs to accelerate data processing, but most of them blindly stack GPUs or blindly increase the number of threads, which not only leads to a linear increase in the processing time of requests, but also fails to improve the system throughput. In response to the drift problem caused by high-speed imaging, some researchers use image algorithms to correct images, although the image quality is improved to a certain extent, but for the high-speed swept-source endoscopic OCT, the speed often exceeds 10,000 rpm/min, the number of axial scans per second exceeds 1,000,000 times. Under such high-throughput data, it is difficult to effectively solve problems, such as image dragging and drifting by algorithmic improvement alone. For the above reasons, this research plans to use the Half-Sync/Half-Asyn mode to optimize memory to build a high-throughput data thread pool for CPU and GPU. On this basis, a swept-source endoscopic OCT system with a real-time image processing rate of not less than 3MHz is built. At the same time, a rotary scanning position information coding feedback module is designed, which realizes 25ns logic timing control through FPGA 40MHz clock to suppress image drift. This method lays the foundation for the non-destructive, in vivo, staining-free, fast and convenient early tumor diagnosis of high-speed endoscopic OCT.

Conclusions

In this study, we developed a high-speed, real-time SS-OCT system using a hardware-software platform based on GPU and FPGA technology. We also demonstrate consecutive A-scan- processing

rates of 3.52 MHz for SS-OCT and the use of an FPGA to suppress image drift under a 40-MHz clock. The imaging platform could perform real-time data acquisition and image reconstruction for a mouse esophagus and human fingers. This technology could pave the way for ultrahigh-speed OCT imaging for applications in guided microsurgery.

Conflict of Interest

The authors declare that there are no conflicts of interest related to this article.

Authors' Contributions

Jing Lyu drafted manuscript. Lin Ren, Qinying Liu and Yan Wang analyzed and interpreted data. Zhenqiao Zhou and Yueyan Chen acquired the data. Hongbo Jia, Yuguo Tang and Min Li provided study conception and design. All authors read and approved the final version.

ORCID IDs

Jing Lyu: https://orcid.org/0000-0002-2261-317X;
Lin Ren: https://orcid.org/0000-0002-6268-8010;
Qinying Liu: https://orcid.org/0000-0003-1687-1049;
Yan Wang: https://orcid.org/0000-0003-3149-2717;
Zhenqiao Zhou: https://orcid.org/0000-0003-0831-8753;
Yueyan Chen: https://orcid.org/0000-0001-8445-4584;
Hongbo Jia: https://orcid.org/0000-0003-1585-2161;
Yuguo Tang: https://orcid.org/0000-0002-0093-6760;
Min Li: https: //orcid.org/0000-0001-6192-5961.

Funding

This work was supported by Scientific Instrument Developing Project of Chinese Academy of Sciences, Grant/Award Number: GJJSTD20190003; Basic Research Pilot Project of Suzhou(No. SJC2021021) and the Scientific Instrument Developing Project of the Chinese Academy of Sciences, Grant/Award Number: YJKYYQ20200052.

Acknowledgements

The first author Jing Lyu was grateful to Dr. Min Li, Dr. Yuguo Tang, and Dr. Hongbo Jia for very helpful discussions and comments; to Mr. Lin Ren for help in composing and layout editing of the figures.

Ethics Statement

The study has been performed in accordance with the ethical standards of the Chinese Academy of Sciences. During the biological experiment, a series of measures such as anesthesia were taken to reduce the damage to mice. All operations were approved by the experimental animal ethics committee of Suzhou Institute of Biomedical Engineering and Technology, Chinese Academy of Sciences, and meet the requirements of the management methods of experimental animals in Jiangsu Province, China.

Data Availability Statement

We analyzed our data using custom-written software in LabVIEW 2019 (National Instruments), and Visual Studio 2017 (Microsoft). The data that support the findings of this study are available from the corresponding author upon reasonable request. The codes supporting the current study have not been deposited in a public repository but are available from the corresponding author upon request. The code will be available by emailing request to lvjing@sibet.ac.cn

References

1) Huang D, Swanson EA, Lin CP, Schuman JS, Stinson WG, Chang W, Hee MR, Flotte T, Gregory K, Puliafito CA, Fujimoto JG. Optical coherence tomography. Science 1991; 254: 1178-1181.
2) Fercher AF, Drexler W, Hitzenberger CK, Lasser T. Optical coherence tomography-principles and applications. Rep Prog Phys 2003; 66: 239.
3) Tearney GJ, Boppart SA, Bouma BE, Brezinski ME, Weissman NJ, Southern JF, Fujimoto JG. Scanning single-mode fiber optic catheter–endoscope for optical coherence tomography. Opt Lett 1996; 21: 543-545.
4) Gora MJ, Suter MJ, Tearney GJ, Li X. Endoscopic optical coherence tomography: technologies and clinical applications. Biomed Opt Express 2017; 8: 2405-2444.
5) Seitz U, Freund J, Jaeckle S, Feldchtein F, Bohnacker S, Thonke F, Gladkova N, Brand B, Schröder S, Soehendra N. First in vivo optical coherence tomography in the human bile duct. Endoscopy 2001; 33: 1018-1021.
6) Winkelmann JA, Eid A, Spicer G, Almassalha LM, Nguyen TQ, Backman V. Spectral contrast optical coherence tomography angiography enables single-scan vessel imaging. Light Sci Appl 2019; 8: 1-9.
7) Wang P, Chen Z, Xing D. Multi-parameter characterization of atherosclerotic plaques based on optical coherence tomography, photoacoustic and viscoelasticity imaging. Opt Express 2020; 28: 13761-13774.
8) Li Y, Jing J, Heidari E, Zhu J, Qu Y, Chen Z. Intravascular optical coherence tomography for characterization of atherosclerosis with a 1.7 micron swept-source laser. Sci Rep 2017; 7: 1-6.
9) Mavadia-Shukla J, Fathi P, Liang W, Wu S, Sears C, Li X. High-speed, ultrahigh-resolution distal scanning OCT endoscopy at 800 nm for in vivo imaging of colon tumorigenesis on murine models. Biomed Opt Express 2018; 9: 3731-3739.
10) Qi L, Zheng K, Li X, Feng Q, Chen Z, Chen W. Automatic three-dimensional segmentation of endoscopic airway OCT images. Biomed Opt Express 2019; 10: 642-656.
11) Li Y, Zhu Z, Chen JJ, Jing JC, Sun CH, Kim S, Chung PS, Chen Z. Multimodal endoscopy for

colorectal cancer detection by optical coherence tomography and near-infrared fluorescence imaging. Biomed Opt Express 2019; 10: 2419-2429.

12) Adams DC, Pahlevaninezhad H, Szabari MV, Cho JL, Hamilos DL, Kesimer M, Boucher RC, Luster AD, Medoff BD, Suter MJ. Automated segmentation and quantification of airway mucus with endobronchial optical coherence tomography. Biomed Opt Express 2017; 8: 4729-4741.

13) Wu T, Cao K, Wang X, Pan R, Huo W, Wang J, He C, Lu Y, Liu Y. Single input state, single mode fiber based spectral domain polarization sensitive optical coherence tomography using a single linear-in-wavenumber spectral camera. Opt Laser Eng 2020; 127: 105948.

14) White BR, Pierce MC, Nassif N, Cense B, Park BH, Tearney GJ, Bouma BE, Chen TC, De Boer JF. In vivo dynamic human retinal blood flow imaging using ultra-high-speed spectral domain optical Doppler tomography. Opt Express 2003; 11: 3490-3497.

15) Liu G, Qi W, Yu L, Chen Z. Real-time bulk-motion-correction free Doppler variance optical coherence tomography for choroidal capillary vasculature imaging. Opt Express 2011; 19: 3657-3666.

16) Nguyen TH, Ahsen OO, Liang K, Zhang J, Mashimo H, Fujimoto JG. Correction of circumferential and longitudinal motion distortion in high-speed catheter/endoscope-based optical coherence tomography. Biomedical Opt Express 2021; 12: 226-246.

17) Klein T, Huber R. High-speed OCT light sources and systems. Biomed Opt Express 2017; 8: 828-59.

18) Fechtig DJ, Grajciar B, Schmoll T, Blatter C, Werkmeister RM, Drexler W, Leitgeb RA. Line-field parallel swept source MHz OCT for structural and functional retinal imaging. Biomed Opt Express 2015; 6: 716-735.

19) Klein T, Wieser W, Eigenwillig CM, Biedermann BR, Huber R. Megahertz OCT for ultrawide-field retinal imaging with a 1050nm Fourier domain mode-locked laser. Opt Express 2011; 19: 3044-3062.

20) Raju P, Justin V M, Daniel M. S, John S. W, Iwona G. Challenges and advantages in wide-field optical coherence tomography angiography imaging of the human retinal and choroidal vasculature at 1.7-MHz A-scan rate. J Biomed Opt 2017; 22: 106018.

21) Xu J, Wei X, Yu L, Zhang C, Xu J, Wong KK, Tsia KK. High-performance multi-megahertz optical coherence tomography based on amplified optical time-stretch. Biomed Opt Express 2015; 6: 1340-1350.

22) Huang D, Li F, He Z, Cheng Z, Shang C, Wai PK. 400 MHz ultrafast optical coherence tomography. Opt Lett 2020; 45: 6675-6678.

23) MacDougall D, Farrell J, Brown J, Bance M, Adamson R. Long-range, wide-field swept-source optical coherence tomography with GPU accelerated digital lock-in Doppler vibrography for real-time, in vivo middle ear diagnostics. Biomed Opt Express 2016; 7: 4621-4635.

24) Wei X, Camino A, Pi S, Hormel TT, Cepurna W, Huang D, Morrison JC, Jia Y. Real-time cross-sectional and en face OCT angiography guiding high-quality scan acquisition. Opt Lett 2019; 44: 1431-1434.

25) Chen C, Shi W, Yang VX. Real-time en-face Gabor optical coherence tomographic angiography on human skin using CUDA GPU. Biomed Opt Express 2020; 11: 2794-2805.

26) Huang Y, Liu X, Kang JU. Real-time 3D and 4D Fourier domain Doppler optical coherence tomography based on dual graphics processing units. Biomed Opt Express 2012; 3: 2162-2174.

27) Kim S, Crose M, Eldridge WJ, Cox B, Brown WJ, Wax A. Design and implementation of a low-cost, portable OCT system. Biomed Opt Express 2018; 9: 1232-1243.

28) Migacz JV, Gorczynska I, Azimipour M, Jonnal R, Zawadzki RJ, Werner JS. Megahertz-rate optical coherence tomography angiography improves the contrast of the choriocapillaris and choroid in human retinal imaging. Biomed Opt Express 2019;10: 50-65.

29) Choi DH, Hiro-Oka H, Shimizu K, Ohbayashi K. Spectral domain optical coherence tomography of multi-MHz A-scan rates at 1310 nm range and real-time 4D-display up to 41 volumes/second. Biomed Opt Express 2012; 3: 3067-3086.

30) Wieser W, Draxinger W, Klein T, Karpf S, Pfeiffer T, Huber R. High definition live 3D-OCT in vivo: design and evaluation of a 4D OCT engine with 1 GVoxel/s. Biomed Opt Express 2014; 5: 2963-2977.

31) Jian Y, Wong K, Sarunic MV. Graphics processing unit accelerated optical coherence tomography processing at megahertz axial scan rate and high resolution video rate volumetric rendering. J Biomed Opt 2013; 18: 026002.

32) Ahsen OO, Lee HC, Giacomelli MG, Wang Z, Liang K, Tsai TH, Potsaid B, Mashimo H, Fujimoto JG. Correction of rotational distortion for catheter-based en face OCT and OCT angiography. Opt lett 2014; 39: 5973-5976.

33) Mavadia-Shukla J, Zhang J, Li K, Li X. Stick-slip nonuniform rotation distortion correction in distal scanning optical coherence tomography catheters. J Innovative Opt Health Sci 2020; 13: 2050030.

34) Nguyen TH, Ahsen OO, Liang K, Zhang J, Mashimo H, Fujimoto JG. Correction of circumferential and longitudinal motion distortion in high-speed catheter/endoscope-based optical coherence tomography. Biomed Opt Express 2021; 12: 226-246.